Fabrication, Characterization and Application of The Water Hyacinth Biochar-Polyvinyl Alcohol Composite as an Advantageous Sound Absorber Material

Pratama Jujur Wibawa (✉ pratamajw@live.undip.ac.id)
  Diponegoro University
Nur Farida Grafiana
  Diponegoro University
Gunawan Gunawan
  Diponegoro University

Abstract

The research was aiming to investigate the potency of water hyacinth (WH) biochar as the most advantageous sound absorber composite when it was blended with polyvinyl alcohol (PVA). Analysis and characterization of the produced WH biochar were essentially performed using N2 absorption-desorption, FTIR spectrophotometer, and SEM methods. While the capability of the sound absorber material was technically conducted using a polyvinylchloride (PVC) impedance tube of about 95 cm in length with internal and outer diameters of about 9.5 cm and 9.8 cm respectively. The materials that would be tested for their capability of sound absorber were prepared in a disk-like form with about 9.5 cm in diameter and 0.5 cm in thickness. The sound source was continuously turned on for 2 minutes and transmitted wirelessly through the impedance tube, and the decreasing intensity of the sound was recorded every 5 seconds. The results showed that the sound absorption coefficient (SAC) of the WH biochar-PVA composite was about 6.50% (0.0650) up to 21.03% (0.2103), while the SAC of the Styrofoam was just about 4.37% (0.0437). This research concluded that the WH biochar produced by the thermal energy of 500ºC indicated it could be the best sound absorber composite when it was blended with PVA, especially for a low frequency of about 440 Hz.

1. Introduction

Water hyacinth (WH) *(Eichhornia crassipes)* is a free-floating invasive aquatic plant that grow and reproduce quite fast in a fresh water containing suitable nutrients. The most favorable aquatic medium for the optimum growth of the WH plant is nutrient-rich water, temperature range of the medium is about 28–30ºC, pH of 6.5 – 8.5, salinity is less than 2%, and trace elements of mineral of N, P, and K is about 20 mg/dm^3, 3 mg/dm^3, and 53 mg/dm^3 respectively. In this condition, the WH plant would be doubles itself within 5–15 days [1]. The natural availability of the WH plants, renewable in properties, and very easy in cultivating for enormous huge quantity leads it to become an advantageous raw material resource for the manufacturing industries producing the renewable material-based industrial products. Due to cellulose, hemicellulose, and lignin are the major composition of WH plants [2–4] therefore manufacturing industry that produce biochar materials-based products would become the most feasible one to be established. Research on the production of WHBC-based biochar composite for sound absorber then becomes very important to be accomplished, and this moment might be the first time it was performed.

The above idea was essentially inspired that any sound of loud enough and lasts long enough to penetrate humans' ears can damage hearing and lead to hearing loss [5]. In general, sounds above 85 decibels (dB) are harmful for human's ears. In this context, people who work with loud machines, vehicles, or power tools, such as construction workers, factory workers, truck drivers, mechanics, or airport ground crew workers are regularly exposed to harmful noise. Besides, military personnel, traffic police, firefighters, and musicians may also be regularly exposed by the harmful noise. To overcome this danger someone needs to wear a sound protector, or the associated sound source was totally covered using a sound absorber material.

Currently, many sound absorber materials have been intensively studied and commercially mass scale produced. Those are commonly made from non-renewable sources such as mineral wool, polyurethan and melamine foams, fiber glass or glass wool [6], recycle tire rubbers [7–9], wood chip [10], natural fibers [11–13], cellulose-based materials [14], and so on. Such materials have high sound absorption coefficient (SAC) but several of those are not environmentally benign. All the sound absorbers aforementioned were basically designed as a panel with a certain shape, size, and thickness by creating an orderly many perforates in the body. Other designs were performed by means of creating layers of the materials with a certain distance between them [5,15,17–20]. Air space, namely cavity generated between layers of the material sheets as well as between holes in the perforated materials mentioned would absorb the sound energy and cut off its propagation. This phenomenon conveys that the porous materials would have similar properties with each other in facilitating sound transmission, they would absorb the sound energy, and at coincident cut off its propagation. It is because the porous materials also belong to so many cavities, namely pores in the micro, meso, and macroscale sizes.

In this relation, activated carbon has widely known that it is one of porous materials that has high surface area up to 2500 m^2/g and high micropore volume up to 1.6 cm^3/g [21–22] so it can be engineered to be a very attractive sound absorber material. In this case, reference [23] have properly proven the capability of sound absorption of the commercial activated carbon at a low frequency (less than 500 Hz). While, reference [24] have patented the granule activated carbon of approximately 1 mm – 2 mm in size grains for the fabrication of sound absorber materials. In addition, reference [25] have successfully fabricated a sound absorber membrane using activated carbon filler, and recorded that in respect of the capability of sound absorption it is better than that produced without activated carbon. However, the biomass of water hyacinth biochar (WHBC) has not been yet employed to fabricate sound absorber materials including by the previous researchers mentioned above. Therefore, this paper comprehensively describes the fabrication of WHBC and investigated its potency as the most advantageous sound absorber material when it was made to become a composite with PVA. The low frequency of about 440 Hz which is equivalent to about 84 decibels (dB) in sound intensity was employed to confirm the capability of sound absorption of the fabricated WHBC-PVA composite. Here, the most important parameter of the capability of sound absorption, *i.e.* SAC was adopted to evaluate the quality of the fabricated WHBC-PVA composite as a sound absorber material. Besides, it also describes the correlation between the capability of sound absorption of the WHBC-PVA composite, its surface morphology, and pore volume distribution. Finally, this paper also proposes the mechanism of the sound absorption process that happened in the fabricated WHBC-PVA composite.

2. Experimental Section

2.1. Materials

Water hyacinth plants from Rawa Pening, Tuntang, Central Java Indonesia. Distilled water (Local laboratory product), Polyvinyl alcohol (PVA), p.a (Sigma Aldrich, USA), "Rajawali" Wood adhesive (Mikatasa Agung, Indonesia); "Tangit" PVC-U adhesive (Henkel, Thailand).

2.2. Instrumentation

Glass tools commonly available in the research laboratory (Pyrex, USA), Hot plate (IKA 3582600 IKA C-MAG MS10, Merk, Germany); Clay-carbonization reactor (Local laboratory product); Electrical Furnace with accessories (Faithful SX4-2-12, China); Electrical oven (Cosmos CO-9919, Indonesia); Plant tissue milling machine (5000 Philips Blender Core HR2221/00, Indonesia); Modified impedance tube (Local laboratory product)(PVC pipe of 95 cm in length, 9.8 cm in outer diameter, 9.5 cm in inner diameter; 440 Hz Sound frequency generator software (Free access from Google Play Store version 3.0, Developer application: LuxDelux, San Fransisco, USA); Sound intensity (dB) recorder software (Fee access from Google Play Store); Bluetooth sound speaker (Frequency response: 90 Hz-200 kHz, Kingstone Model K-9, Shenzhen, China); Thermal gravimetry analysis (TGA) (Netzsch STA 409 CD, Germany); N_2 adsorption-desorption Brunauer-Emmett-Teller and Barrett-Joyner-Halenda (BET-BJH) analysis (Quantachrome Instrument 3.01, USA); Fourier-transformed infrared (FTIR, Perkin Elmer Spectrum Version 10.4.00, USA); Scanning electron microscope-Energy dispersive X-ray spectroscopy (SEM-EDX, JEOL JSM-6510L, Japan).

2.3. Procedure

2.3.1. Fabrication of the WHBC-PVA composite disk

Firstly, about 600 g water hyacinth (WH) plants of approximately 3 cm length cut was dried-up under sunlight exposure for 7 days to reach the moisture content of ~ 1%. The dried WH obtained was then properly milled to transform it becomes WH fine powder of 100 mesh (~ 149 μm) in particles size, and subsequently it was carbonized using a closed clay-carbonization reactor at 110°C for 30 minutes. To avoid ash-like material generation during the carbonization process, needs water spray treatment when fire appeared for getting biochar. A half-part of the produced biochar was then heated at various temperatures of 400, 500 and 600°C using an electrical furnace equipped with 10 cm^3/minutes nitrogen (N_2) gas flow. After that, about 16 g of the obtained biochar was blended properly with 100 cm^3 polyvinyl alcohol (PVA) of 1 % weight/volume (w/v) until a gel-like viscous liquid formed. This mixture was then gently poured into a cylindrical mold of 0.5 cm thick, and 9 cm internal diameter, flatting the surface manually, and let dry in an electrical oven set up at 110 °C for 24 hours. These products were then labeled as WHBC400, WHBC500 and WHBC600 for the water hyacinth biochar obtained from 400, 500 and 600°C heating temperatures respectively.

2.3.2. Fabrication of water hyacinth (WH)-PVA disk

About 1000 g of the water hyacinth (WH) plant obtained from a Lake Rawapening (Semarang, Indonesia) was washed with fresh water and then dried under sunlight exposure at ambient temperature and pressure for about 6 days. Subsequently, the dried WH plant was then chopped to smaller sizes slices of about 3−5 cm in length and crushed to become micro-powder of about 100 mesh using a blender machine. After that, about 16 g the WH powder was mixed properly with 100 cm^3 PVA of 10% w/v until a gel-like viscous liquid formed. This mixture was then gently poured into a cylindrical mold of 0.5 cm thick and 9 cm internal diameter, flatting the surface manually, and let dry in an electrical oven set up at 110 °C for 24 hours.

2.3.3. Analysis and characterization

Typical functional groups, surface morphology, and surface area as well as total pore volume of the fabricated WHBC-PVA composites were analyzed by using FTIR spectrophotometry, SEM and nitrogen (N_2) gas adsorption-desorption Brunauer-Emmett-Teller method respectively. On the other hand, the porosity of the WHBC-PVA composite could be approximately evaluated based on the common definition of porosity of solid materials, *i.e.* total volume of the generated voids divided by the volume of its total mass [26]. In this context, the total volume of voids was equal to the volume of total mass and was subtracted by the total pore volume obtained from the multi-points isotherm BET analysis. Total mass volume of the material could be calculated from the mass of the associated material divided by its density. In this relation, the density of the fabricated WHBC-PVA composite disk could be determined according to an equation of $\rho = m/V$ where ρ is density, m and V is mass and volume of the fabricated WHBC-based material disk, respectively. Here, the volume of the fabricated WHBC-PVA composite disk could be calculated by means of the thickness of the associated WHBC-PVA composite disk, *i.e.* 5 mm, multiplied by πr^2 where π is constant number of 3.1429, and r is radius of the WHBC-PVA composite disk mentioned. Thus, porosity of the fabricated WHBC-PVA composite disk could be determined according to the equation of $\Phi = V_1/V_2$ where Φ is porosity, V_1 and V_2 is total volume of voids, *i.e.* interparticle pore, and that of the mass of the WHBC-PVA composite disk respectively. In this case, V_1 would be equivalent to V_2 minus total volume of intra particles pores, *i.e.* the pore volume obtained from the BET analysis.

On the other hand, to confirm the existence of several kinds of functional groups which constructed the produced WHBC-PVA composite, it was using FTIR spectrophotometry. In this case, about 1 g WHBC-PVA composite was properly mixed with a few grams of KBr powder and pressed it to form KBr pellet, and put it in a transparent disk. The disk was then heated at 110 °C in an electrical oven to evaporate up any moisture content. Finally, the disk was put in the FTIR sample holder and carefully scanned for the 420−4000 cm^{-1} wave number spectra. The last was surface morphology analysis of the WHBC-PVA composites using SEM. In this case, the WHBC-PVA composites each was independently deposited on a clean glass wafer of 1 cm · 1 cm in size, then coated it with platinum (Pt) sputtering. The instrument was run on high vacuum mode (HV), 20kV employing both a secondary electron (SE) detector and backscattered electron detector (BSED) to explore the best surface morphology of the analyzed samples.

2.3.4. The capability of sound absorber test

The capability of sound absorber test of the fabricated WHBC-PVA composite was performed by using an impedance tube as schematically depicted in Fig. 1.

The impedance tube shown in Fig. 1 was assembled according references [27−30] with a little bit modification. As it can be seen in Fig. 1, the sound frequency generator was marked as (1), while the Bluetooth sound speaker was mark as (2), the impedance tube body was marked as 3, then the tested sample of WHBC materials (marked 4) was carefully pushed into the impedance tube using a sample holder stick (marked 5 and 6) until a point that located at about 41 cm away from the sound speaker, 2. In this research, the sound speaker could catch and transmit the sound intensity came wirelessly from the sound generator of 440 hertz 1. Here, the capability of a sound absorber would be equivalent to the number of sound transmission losses that could be recorded by a Sound meter software (marked 7), expressed in decibel (dB) or hertz (Hz).

The fabricated WHBC-PVA composite tested (0.5 cm in thickness; 9.5 cm in diameter) was fixed placed in the impedance tube about 41 cm far away from the sound speaker, while the sound generator frequency employed was 440 Hz displayed as 84 dB. The reduced sound frequency or sound intensity was then recorded by a sound meter, the testing was performed for 2 minutes with every 5 seconds the sound-reducing was documented. In addition, Styrofoam aerosol was used as a positive control of the sound absorber material, while original WH powder mixed with wood glue, and with polyvinylchloride (PVC)-based materials as comparations, and then they are encoded as WH$_{ori}$1, and WH$_{ori}$2 respectively.

3. Result And Duscussion

3.1. The WHBC-PVA composite products

Several products of the WHBC-PVA composites disks produced in this research were displayed in Fig. 2.

3.2. Surface Area and Pores Analysis

The results of the surface area and pore volume analysis of the fabricated WHBC400-PVA, WHBC500-PVA, and WHBC600-PVA composites were displayed in Table 1. The original data shown in Table 1 were generated by the Quantachrome Instruments version 3.01, and it was placed in the Supplementary Information file of S1 up to S6, and its summary is shown in Table S1_S2 (BET Summary of the isotherm multi-point BET analysis) and Table S3_S4_S5_S6 (Summary of the BJH adsorption-desorption analysis).

Table 1
Summary of the isotherm multi point BET and BJH analyses of the WHBC-PVA composites

| Composites | w/ g | Isotherm BET Adsorption-Desorption Analysis | | | | | | Isotherm BJH Analysis | | | |
| | | | | | | | | Adsorption | | | Desorption |
		s	i	W_m/ g	C	SA_{tot}/ m² g⁻¹	SA_{sp}/ m² g⁻²	SA_p/ m² g⁻¹	V_p/ cm³ g⁻¹	r_p/ Å	SA_p/ m² g⁻¹
WHBC400-PVA	0.0814	114,200.00	24,110.00	7.23014E-06	5,737.00	25,179.00	309,324.32	16,260.00	0.033	15,291.00	16,164.00
WHBC500-PVA	0.0833	167,891.00	19,600.00	5.33359E-06	9,568.00	18,575.00	222,989.20	14,512.00	0.035	15,620.00	13,360.00
WHBC600-PVA	0.0816	101,482.00	25,720.00	7.86151E-06	4,945.00	27,378.00	335,514.71	19,915.00	0.045	17,032.00	22,359.00

w: sample weight in gram; s: slope; i: intercept; W_m: 1/(s + i) is adsorbed adsorbate weight monolayer in gram; C: 1/(W_m*i) is a BET constant; SA_{tot}: total surface area; SA_{sp}: specific surface area; m: meter; g: gram; SA_p: pore surface area; r_p :pore radius; .

Table 1 shows the total surface area and specific surface area of the fabricated WHBC600-PVA is the largest one compared to the others, i.e., 27,378.00 m² g⁻¹ and 335,514.00 m² g⁻¹ respectively. These facts demonstrated that the higher pyrolysis temperature could enlarge not consistently the surface area of WHBC-PVA composite. As shown in Table 1, the surface area of the fabricated WHBC400-PVA, WHBC500-PVA and WHBC600-PVA increases significantly from 25,179.00 to 27,378.00 m² g⁻¹ due to pyrolysis proses conducted at 400 to 600°C respectively, but it decreased became 18,575.00 m² g⁻¹ when it was pyrolyzed at 500°C, so does its specific surface area.

Comparing pore volume of the adsorption and desorption analysis we know that not all the adsorbed nitrogen was desorbed again, but a part of them condensed in the pores of the fabricated WHBC-PVA composites. According to reference [34], the nitrogen condensation would just occur in the typical pores of cylindrical in shape and mesopores in size. Thus, the typical pore of the fabricated WHBC-PVA composites could be classified into cylindrical pore in shape and mesopores (2 – 50 nm) in size. This situation of the nitrogen condensation leads the pores volume to become smaller during the nitrogen adsorption-desorption process. As we can see in Table 1, the pore volume of the fabricated WHBC400-PVA composite decreases from 0.033 cm³g⁻¹ (adsorption) to 0.031 cm³g⁻¹ (desorption); so, does that of WHBC500-PVA decreases from 0.035 cm³g⁻¹ to 0.033 cm³g⁻¹; and WHBC600-PVA decreases from 0.045 cm³ g⁻¹ to 0.042 cm³g⁻¹. It means about 0.002 cm³g⁻¹ (6.06%) nitrogen condensed in the pores of the WHBC400-PVA as well as the WHBC500-PVA, and 0.003 cm³g⁻¹ (6.67%) nitrogen condensed in the pores of WHBC600-PVA composite. The condensation happened due to the capillary forces working inherently in the pore of 2–50 nm in size [34]. However, from the chemistry point of view, the nitrogen condensation happened due to the presence of the nitrogen-withdrawing functional groups which constructed the inside wall of the associated pores. These functional groups always vibrate alongside their covalently atomic bonds so that the nitrogen molecules could be properly trapped between the vibrating bonds closer to each other. We can imagine the work of such vibration in trapping nitrogen is similar to the work of molecular sieves, or more clearly similar to the work of filter paper.

In correlation to the IUPAC classification of the isotherm adsorption types [32–33], the curves correlated the quantity of the adsorbed nitrogen (STP, cm³) against relative pressure (P/P$_o$) happened on the aforementioned WHBC-based materials have been properly drawn as shown in Fig. 3. In relation to that, the original curve of the automated gas sorption data released by the Quantachrome Instruments version 3.01 was displayed in Supplementary Information, S7.

Figure 3 shows all the pores of the WHBC-PVA composites approximately fit to the H3 type hysteresis loop in adsorption-desorption properties. According to references [32, 33, 35] this typical hysteresis is generated by non-rigid aggregates of plate-like particles, and the particles subsequently generated voids of slit-

shaped pores. It means that the particles of the WHBC-PVA composites themselves might be nonporous or macro-porous adsorbent as their properties also very match with type II of the IUPAC classification of isotherm adsorption pores. Thus, the pore radius displayed in Table 1, are very varies depends on the typical material and the sorption process. It can be well known that the diameter of the pores aforementioned ranging from about 30–36Å (3–3.6 nm), and then they could be identified as mesopores. This situation indicated that the pores throughout constructed the macro-porous of the WHBC-PVA composites, actually are voids, i.e., inter particles pores with more than 50 nm in size. It becomes reasonable if the voids aforementioned might have temporally adsorbed nitrogen gas and subsequently infiltrate into the most suitable mesopores. Finally, the adsorbed nitrogen gas condensed in it during the adsorption-desorption equilibrium process at every value of relative pressure, P/Po due to the capillary forces.

Combination of the macro-voids and mesopores which simultaneously construct the WHBC-PVA composites lead to the formation of multilayer nitrogen gas adsorbate adsorbed on the surface of the associated materials. It matches with type II of the IUPAC classification of isotherm adsorption.

3.3. Functional groups analysis

The functional groups analysis of the fabricated WHBC-PVA composites result performed using FTIR spectroscopy is displayed in Fig. 4. The original FTIR spectra data of the WHBC-PVA composites aforementioned was presented in Supporting Information of the FTIR spectra data Microsoft Excel format. Figure 4 shows six wavenumber peaks located at around 3428, 1721, 1625, 1209, 1040, and 876 cm^{-1} were generated by original WHBC (WHBCori)(Fig. 4(d)). The FTIR spectra pattern demonstrated that the wavenumber peaks of 1721 cm^{-1} and 1209 cm^{-1} disappeared on the WHBC that produced by pyrolysis temperature at 400, 500, and 600°C before it was blended with PVA as shown in Fig. 4(a), 4(b), and 4(c).

Referring several references [36–38], wavenumber peaks of 3428 cm^{-1} represents O-H stretch of dimetric (single bridge compounds) or O-H stretch of aliphatic alcohol (R-OH), or aromatics-OH intramolecular hydrogen bond. It clearly confirmed that the such -OH group comes from PVA forming the composite of WHBC-PVA aforementioned. While, the wavenumber peaks of 1721 cm^{-1} represents C = O stretch of saturated aliphatic acid, or C = O of ketone. It confirmed that the carbonaceous molecular structure of the original WHBC consisted of C = O group, one of them. Later on, the C = O group would have been used to gain PVA molecules through their OH group formed hydrogen bonding of which unite them become a composite, namely WHBC-PVA composite. Furthermore, wavenumber peaks of 1625 cm^{-1} represents alkenyl C = C stretch or aryl substituted C = C or conjugated C = C. While, wavenumber peaks of 1417, 1209, 1040, and 876 cm^{-1} represents C = C-C aromatics rings stretch, aromatics C-H in plane blend, cyclohexane ring vibration, and aromatic C-H out of plane blend respectively. That all demonstrated and made sure that basically the molecular structure framework of the WHBC-PVA composites constructed by several units of carbon-carbon single bond and double bond, aromatic, and cyclohexane ring, of which all of them were covalently jointed each other so that forming a framework of a material of WHBC-PVA composite. This assignment of the FTIR spectra above can be then summarized such as in Table 2. These data indicated that several important functional groups are still present in the WHBC-PVA composites of WHBC400-PVA, WHBC500-PVA, and WHBC600-PVA.

Table 2
Summary of the assignment of the FTIR spectra wavenumber peaks of which is displayed in Fig. 4

Wave number/ cm^{-1}		Assignment of the atomic bond's representatives	Cited references
This paper	Reference		
3428	3550 – 3450	O-H stretch of dimetric (single bridge compounds)	[36, 37]
	3595 – 3425	O-H stretch of R-OH, Ar-OH intramolecular hydrogen bond	[36]
1721	1725 – 1700	C = O stretch of saturated aliphatic acid, dimer, acyclic)	[36, 37]
	1720 – 1700	C = O of ketone, 6 rings	[36]
1625	1680 – 1620	Alkenyl C = C stretch.	[36, 37]
	1625	Aryl substituted C = C	[36]
	1600	Conjugated C = C	[36]
1417	1510 – 1450	C = C-C aromatics rings stretch	[36, 37]
1209	1225–950 (several)	Aromatics C-H in plane blend	[36, 37]
1040	1055 – 1000	Cyclohexane ring vibration	[36]
876	900–670 (several)	Aromatic C-H out of plane blend	[36–38]

3.4. Surface morphology analysis

Surface morphology of the fabricated WHBC-PVA composites explored with SEM are displayed in Fig. 5. We can see in Fig. 5 surface morphology of the fabricated WHBC-PVA composites are quite different each other, and all did not show a regular pattern.

From the molecular stability point of view, the thermal energy of 500°C equivalent might have caused the hydrocarbon molecular framework conformation got the most stable. The evidence of the stability of the molecular framework was convincingly demonstrated by appearing FTIR spectra of wavenumber peak of 876 cm^{-1} as shown in Fig. 4(b). The wavenumber peak of 876 cm^{-1} represents aromatic C-H out of plane bend [36, 37] so if this spectrum is still generated it means that the aromatics moieties of the hydrocarbon molecular framework did not collapse under the thermal energy exposure of about 500°C.

3.5. Sound absorption analysis

Results of the reducing sound intensity test was displayed in Table 3. While, the print screen of the recorded decreasing sound intensity released by the employed Sonometer software was displayed in Supplementary Information, S8 up to S14, and the summary of decreasing intensity of the sound was shown in Table S9_S14. We can see in Table 3 that the fabricated WHBC-PVA composite produced through thermal activity at 500°C encoded as WHBC500-PVA composite provided the best capability of sound adsorber of which represented by sound absorption coefficient (SAC) of about 21.03% or 0.2103.

Table 3
Sound absorption coefficient of the fabricated WHBC-PVA composites, the frequency of the sound incident was 440 Hz, that was expressed as 84 dB in intensity

Material	Density/ g cm^{-3}*	Porosity/%**	Duration of the sound on/minutes	Sound intensity decreased (I_d) in average after passed through the associated materials in average / dB	Sound intensity absorbed (I_a)/ dB***	Sound absorption capacity, ⊠/dB minute^{-1} ****	Sound absorption coefficient, ψ/ %*****
Without adsorbent	n.a	n.d	2	84.0000 ± 0.0000	0.0000	0.0000	0.00
Styrofoam	0.0137	n.d	2	80.3333 ± 1.0072	3.6667	1.8334	4.37
WH$_{ori}$1	0.2074	n.d	2	73.4167 ± 0.7755	10.5833	5.2917	12.60
WH$_{ori}$2	0.2065	n.d	2	78.0833 ± 0.9286	5.9167	2.9584	7.04
WHBC400-PVA	0.3845	98.64	2	76.3750 ± 0.8242	7.6250	3.8125	9.08
WHBC500-PVA	0.3888	98.59	2	66.3333 ± 1.1293	17.6667	8.8334	21.03
WHBC600-PVA	0.3935	98.17	2	78.1667 ± 0.7614	5.8333	2.9167	6.94
*n. a: not available; n. d: not determined.							
**Calculated with equation of reference [26], i.e., Φ = (V_v/V_m) where V_v and V_m is total volume of voids, and total volume of the mass of the materials, respectively							
***Calculated with equation of $I_a = (I_i - I_f)$ where I_a, I_i and I_f is sound intensity absorbed, intensity of the sound incident, and final intensity of the sound after passed through the materials respectively.							
****Calculated with equation of = I_a/S_t where , and S_t is sound absorption capacity, and duration of the sound to on respectively.							
*****Calculated with equation of ψ = [(84 - I_d)/84]·100% or ψ = (I_a/84)·100%, where ψ is sound absorption coefficient, and 84 means 84 dB that is sound intensity without adsorbent							

Here the SAC was calculated according the definition of the SAC, i.e. the ratio of sound energy absorbed to the sound energy incident, where the value would be 0 (not absorbed at all) up to 1 (totally absorbed) [27–30]. In this context, we propose the term sound absorption capacity (SACap) encoded as   and defined as the intensity of the sound absorbed during the sound absorption process happening for a certain time determined. By the definition of SACap aforementioned, we can also see in Table 3 that the material encoded as WHBC500-PVA has the best capability of sound absorber since the SACap of it was highest, i.e., 8.8334 dB minute^{-1}.

The value of both SAC and SACap of the WHBC500-PVA is higher than that of the commonly used sound absorber material, Styrofoam, which is just 4.37%, and 1.8334 dB minute^{-1} respectively. The value of SAC and SACap of the WHBC500 is also higher than that of original WH powder mixed with PVA adhesive for woods encoded as WHori-PVA-wood (in brief as WH$_{ori}$1), that is about 12.50%, and 5.2500 dB minute^{-1} respectively. Also, the value of SAC and SACap of the WHBC500-PVA is also higher than that of the original WH powder mixed with PVA adhesive for PVC encoded as WHori-PVA-pvc (in brief as WH$_{ori}$2), which is just 6.99%, and 2.9375 dB minute^{-1} respectively. The facts above convincingly prove that WH that heated at 500°C and form biochar (bio-charcoal) powder would be so much better sound absorber material compared to the original WH. Nevertheless, the most interesting is all of the fabricated WHBC-PVA composites aforementioned possessed the SAC as well SACap higher than the commonly used sound absorber material, Styrofoam.

Another interesting is when we compare the SAC of the fabricated WHBC500-PVA composite with that of other sound absorber materials of paper sludge-cemented composite, wool, jute, and polystyrene materials reported by several previous researchers [39–41]. Based on the SAC of each material aforementioned, the capability of sound absorption of the WHBC500-PVA composite is little bit better than all the materials mentioned as shown in Table 4. As we can see in

Table 4
Sound absorption coefficient (SAC) of some porous materials

Sound Incident	Material	SAC	References*
400 Hz	Styrofoam	0.044	This paper
s.a.a	$WH_{ori}1$	0.125	s.a.a
s.a.a	$WH_{ori}2$	0.070	s.a.a
s.a.a	WHBC400-PVA	0.091	s.a.a
s.a.a	WHBC500-PVA	0.210	s.a.a
s.a.a	WHBC600-PVA	0.069	s.a.a
125−500 Hz	Paper slude-cemented composite	0.05−0.3	[42]
250−1600 Hz	Paper slude-clay composite	0.550	s.a.a
400 Hz	Micro-perforated panel hexagonal shape-based Jute system	0.810	[5]
400 Hz	Micro-perforated panel circle shape-based Jute system	0.850	s.a.a
400 Hz	Micro-perforated panel spiral shape-based Jute system	0.790	s.a.a
500 Hz	Cotton	0.500	[39−41]
s.a.a	Ramie	0.400	s.a.a
s.a.a	Wool	0.200	s.a.a
s.a.a	Jute	0.200	s.a.a
s.a.a	Bamboo	0.600	[39, 43]
s.a.a	Kapok	0.570	[39, 44]
s.a.a	Glass wool	0.400	[39]
s.a.a	Mineral wool	0.700	s.a.a
s.a.a	Polystyrene	0.100	s.a.a
*s.a.a : same as above			

Table 4, SAC of the WHAC500-PVA composite (0.21) is bigger than that of paper sludge-cemented composite, i.e., 0.05 [42], wool and jute each is 0.200 [39−41], and polystyrene, i.e., 0.100 [39]. However, the capability of sound absorption of the WHBC500-PVA composite is still lower than the others ones shown in Table 4, for examples such as Micro-perforated panel circle shape-based Jute system (SAC: 0.850), Micro-perforated panel hexagonal shape-based Jute system (SAC: 0.810), Micro-perforated panel spiral shape-based Jute system (SAC: 0.790), and so on. These facts attributed that the most important sound absorption parameters, i.e., closed pores, so the total number of closed pores of the WHBC500-PVA composite might be a few more than paper sludge-cemented composite, wool, jute, and polystyrene materials. Vice versa, the total number of closed pores of the WHBC500-PVA composite might so much lesser than the Micro-perforated panel circle shape-based Jute system, Micro-perforated panel hexagonal shape-based Jute system, Micro-perforated panel spiral shape-based Jute system, and so on.

In relation to the surface morphology of the fabricated WHBC-PVA composites, we can see in Fig. 5 that the shape and size of the smallest particular grains might become the most influential factors for the capability of the sound absorber of the associated materials. In this case, no spherical particles were generated and observed in all the fabricated WHBC-PVA composites including WHBC500-PVA one. The shapes and sizes of particular grains of WHBC500-PVA composite are very varied as stone-like, pipe-like, and plate-like as shown in Fig. 5(b) inset 1, 2, and 3 respectively with about 3−5 μm in size. The particles were randomly agglomerated so that generating inter-particles space (voids) with various shapes, sizes, and depths. The generated voids especially those located under the surface of the materials, namely isolated voids probably have less air content so that the sound could not propagate through the associated materials. The more voids the better the sound absorber. In conjunction with the shape of the particle's grains, the contour of their surface border might also affect the capability of sound absorber. The basins and indentations generated on the surface of the particles could break totally the sound propagation through the associated materials. As it has already widely been known that sound wave propagates by longitudinal mode of propagation. In this point of view, the frequency of the sound wave could be reduced drastically by the basins and indentations aforementioned due to the direction of the sound propagation changing randomly.

Accordingly, it can be underlined that the fabricated WHBC-PVA composites belong to two ways in reducing sound frequency which resulting sound absorption. The first one is through isolated voids especially those no air content or minimum air content. In this situation, the frequency of sound of which represents the number of vibrations per second would be reduced since no any matter or minimum quantity of matter could be vibrated. The second one is through the basins and indentations formed the surface roughness of the particles. In this situation, the frequency of sound would be reduced since the direction of the sound propagation become change to randomly directions depending on the number of basins and indentations as well as the shape, depth, and also directions of them. According reference [31] the basins and indentation turns constructed the surface of an activated carbon-based material particle can be classified into four categories of directions and depths. Those are Q1, Q2, Q3, and Q4 in directions, and sharp turns (θ1), semi sharp turns (θ2), obtuse

turns (θ3), and non-significant turns (θ4) in depths. The Q1, Q2, Q3, and Q4 directions of turns, and sharp turns (θ1), semi shar turns (θ2), obtuse turns (θ3), and non-significant turns (θ4) depths of the turns have been detailly explained in reference [31].

Finally, the reducing frequency of sound propagated through the WHBC-PVA composites including WHBC500-PVA one, namely sound absorber mechanism can be schematically illustrated as in Fig. 6. Figure 6 shows the longitudinal propagations of sound wave that is represented by lines through the materials encoded as WHBC500. The amplitude (A) of the sound wave and its wavelength (λ) do not change during propagation, but frequency (f) is essentially change. In this illustration, the wavelength of the sound incident was constructed by 15 lines (assumed 1 line represents 29 vibrated lines per second approximately, so that 15 lines would be equivalent to 440 Hz), when the sound touches the surface of the outer wall void the quantity of the lines is then reduced became 6 vibrated lines per second (means equal to 174 Hz, approximately). It is because several lines have been reflected back when they touch the wall having basins with various sharp and depths, it means the frequency of the sound decrease from 440 Hz to 174 Hz. Furthermore, 6 vibrated lines existing in the void change become 4 vibrated lines when the sound propagates through into the isolated void with a lesser quantity of air content.

As it has been widely known that the frequency is the amount of vibration per second, so if the sound incident through into a void with a minimum quantity of air surely the sound frequency would be down, in another word the sound was absorbed by the associated material. The proposed mechanism of the sound absorption explained above would be similar with that reported by reference [45].

4. Conclusion

It was clear that the fabricated WHBC-PVA composites can properly absorb sound especially of about 440 Hz in frequency or about 84 dB in intensity. The WHBC-PVA composites of which the WHBC produced by pyrolysis at 500°C would be the best potential sound absorber when it was blended with PVA to become composite of WHBC500-PVA with the highest SAC of about 21.96% (0.22) and SACap of 9.3334 dB minute^{-1}. The value of the SAC as the SACap is so much higher than that of the WHori1 and WHori2, even if it is compared to the Styrofoam material. In this case, the SAC of WHori1, WHori2, and Styrofoam materials was 13.53%, 8.09%, and 5.49% respectively. While, the SACap of WHori1, WHori2, and Styrofoam materials was 5.7500, 3.4375, and 2.3334 dB minite^{-1} respectively. Despite of biochar material form of the WH material connivingly provides the better sound absorber properties compared to the WHori one, but the capability of sound absorption of the WHBC-PVA composites are not significantly correlated with the value of their total surface area and total pore volume of intra particles (obtained from BET analysis). Interestingly, the capability of sound absorption of the WHBC-PVA composites quite correlates with their total volume of voids that is expressed as porosity rather than the volume of intraparticle pores that obtained from BET analysis. In addition, pore radius of intraparticle pores is also influencing the capability of sound absorption rather than pore volume of intraparticle pore. Overall, the higher porosity and pore radius of the fabricated WHBC-PVA composites would have become the better sound absorber materials.

Declarations

SUPPORTING INFORMATION

The relevant data which is related to the sound reductions measurement performed with the free-access sound meter software, original data of pore size distribution, pore-volume, and surface area of the produced materials reported in this research, and are not displayed in this paper has been presented as Supplementary Information file, and it can be accessed freely from the given link of the Journal of Inorganic and Organometallic Polymers and Materials.

CONFLICT OF INTEREST

The authors declare no conflict of interest.

AUTHOR CONTRIBUTION

P.J.W wrote the main manuscript text; N.F.G and G prepared Figure 1, Figure 2 and Figure 3. All authors reviewed the manuscript.

References

1. Dersseh, M. G., Melesse, A. M, and Dagnew, D. C. 2019. Water hyacinth: review of its impacts on hydrology and ecosystem services—Lessons for management of Lake Tana, Chapter 19: Extreme Hydrolysis and Climate Variability: Monitoring, Modelling, Adaptationand Mitigation, Editors: [2] Melesse, A.M., Abtew, W, and Senay, G. page: 237-251. Copyright © 2019 Elsevier Inc. All rights reserved. DOI: 10.1016/C2017-0-04193-9.
2. Keche, D.D., Fetanu, Z. M., Babiso, W. Z., and Wachemo, A. C. 2022. Anaerobic digestion of urea pretreated water hyacinth removed from Lake Abaya; bio-methane potential, system stability, and substance conversion, *RSC Advances*, **12:** 8548. DOI: 10.1039/d2ra00303a.
3. Ilo, O. P., Simatele, M.D., Nkomo, S. L., Mkhize, N.M., and Prabhu, N. G. 2020. The Benefits of Water Hyacinth *(Eichhornia crassipes)* for Southern Africa: A Review, *Sustainability*, **12:** 9222. DOI:10.3390/su12219222.

4. Varanasi, J.L., Kumari, S., and Das, D. 2017. Improvement of energy recovery from water hyacinth by using integrated system, *International Journal of Hydrogen Energy*, **43:** 1303–1318. DOI: 10.1016/j.ijhydene.2017.11.110 0360-3199.

5. El-Basheer, T. M. 2022a, Study on audiometer calibration at the extended high-frequency range 8-16 kHz. *Noise & Vibration Worldwide*, **53(1-2)**, 24-37. DOI: 10.1177/09574565211052691.

6. Ulrich, T. and Arenas, J.P. 2020. Sound absorption of sustainable polymer nanofibrous thin membranes bonded to a bulk porous material, *Sustainability*, **12(6):** 2361. DOI: 10.3390/su12062361.

7. Pfretzschner, J. and Rodriguez, R.M. 1999. Acoustic properties of rubber crumbs. *Polymer Testing*, **18:** 81–92. DOI: 10.1016/S0142-9418(98)00009-9.

8. Swift, M.J.; Briš, P. and Horoshenkov, K.V. 1999. Acoustic absorption in re-cycled rubber granulate. *Applied Acoustic*, **57:** 203–212. DOI: 10.1016/S0003-682X(98)00061-9.

9. Xu, X.; Wang, H.; Sun, Y.; Han, J. and Huang, R. 2018. Sound absorbing properties of perforated composite panels of recycled rubber, fiberboard sawdust, and high density polyethylene. *Journal of Cleaner Production*, **187:** 215–221. DOI:10.1016/j.jclepro.2018.03.174.

10. Boubel, A.; Garoum, M.; Bousshine, S. and Bybi, A. 2021. Investigation of loose wood chips and sawdust as alternative sustainable sound absorber materials. *Applied Acoustics*, **172:** 107639. DOI: 10.1016/j.apacoust.2020.107639.

11. Arenas, J.P.; del Rey, R.; Alba, J. and Oltra, R. 2020. Sound-absorption properties of materials made of esparto grass fibers. *Sustainability*, **12(14):** 5533. DOI: 10.3390/su12145533.

12. Taban, E.; Khavanin, A.; Faridan, M.; Samaei, S.E.; Samimi, K. and Rashidi, R. 2020. Comparison of acoustic absorption characteristics of coir and date palm fibers: Experimental and analytical study of green composites. *International Journal of Environmental Science and Technology*, **17(1):** 39–48. DOI: 10.1007/s13762-019-02304-8.

13. Hakim, A., Awad, E. H., El-Nemr, K. F., & El-Basheer, T. M. 2021. Impact of gamma radiation and multi-walled carbon nanotubes on the mechanical and acoustical properties of reinforced sisal fiber/polyester resin composites. *Radiation Physics and Chemistry*, **189:** 109768. DOI: 10.1016/j.radphyschem.2021.109768.

14. Jahangiri, P.; Logawa, B.; Korehei, R.; Hodgson, M.; Martinez, D.M. and Olson, J.A. 2016. On acoustical properties of novel foam-formed cellulose-based material. *Nordic Pulp and Paper Research Journal*, **31(1):** 14–19. DOI: 10.3183/NPPRJ-2016-31-01-p014-019.

15. Yang, X.; Bai, P.; Shen, X.; To, S.; Chen, L.; Zhang, X. and Yin, Q. 2019. Optimal design and experimental validation of sound absorbing multilayer microperforated panel with constraint conditions. *Applied Acoustics*, **146:** 334–344. DOI: 10.1016/j.apacoust.2018.11.032.

16. Gai, X.L.; Cai, Z.N.; Xing, T.; Wang, F.; Li, X.H.; Zhang, B. and Guan, X.W. 2020. Experimental study on sound absorbing property of spatial absorber of non-woven fabric with micro-perforated plate-like structure. *Applied Acoustics*, **160:** 107156. DOI: 10.1016/j.apacoust.2019.107156.

17. Cobo, P.; de la Colina, C.; Roibás-Millán, E.; Chimeno, M. and Simón, F. 2019. A wideband triple-layer microperforated panel sound absorber. *Composite Structure*, **226:** 111226. DOI: 10.1016/j.compstruct.2019.111226.

18. Maamoun, A. A., El-Wakil, A. A., & El-Basheer, T. M. 2022. Enhancement of the mechanical and acoustical properties of flexible polyurethane foam/waste seashell composites for industrial applications. *Journal of Cellular Plastics*, **58 (4)**: 645-672. DOI: 10.1177/0021955X221088392.

19. El-Basheer, T. M., El Ebissy, A. A., & Attia, N. F. 2022b. Fabrication of cost-effective double layers composite for efficient sound-absorbing based on sustainable and flame-retardant jute fabrics. *Journal of Industrial Textiles*, **51(35)**, 4097S–4117S. DOI: 10.1177/15280837221098197.

20. El-Basheer, T. M., Youssef, R. S., & Mohamed, H. K. 2017. NIS method for uncertainty estimation of airborne sound insulation measurement in field. *International Journal of Metrology and Quality Engineering*, **8(19)**: 1-9. DOI: 10.1051/ijmqe/2017009.

21. Bechwati, F. and Avis, M. R.; Bull, D. J.; Cox, T. J. and Hargreaves, J. A.; Moser, D. and Ross, D. K.; Umnova, O. and Venegas, R. 2012. Low frequency sound propagation in activated carbon, *The Journal of the Acoustical Society of America*, **132(1):** 239–248. DOI: 10.1121/1.4725761.

22. Jiang, N., Chen, J. Y. and Parikh, D. V. 2009. Acoustical evaluation of carbonized and activated cotton nonwovens, *Bioresource Technology*, **100:** 6533–6536. DOI: 0.1016/j.biortech.2008.10.062.

23. Suzuki, M. 1994. Activated carbon fiber: fundamental and applications. *Carbon*, **32(4):** 577–586. DOI: 10.1016/0008-6223(94)90075-2.

24. Bay, K., Leistner, M., Maysenhölder, W. and Leistner, P. 2006. Sound absorber made of activated carbon granulate, *Internationale Patentklassifikation*: G10K 11/165 (2006.01).*Internationale Veröffentlichungsnummer Patent*: WO 2015/004191 AI. *Internationale Veröffentlichungsdatum*: 15.01.2015.

25. Marin, P. and Arenas, J.P. 2019. Sound absorption provided by an impervious membrane/cavity/ activated carbon arrangement, *Proceeding of the 23rd International Congress on Acoustic*, 9-13 September 2019, Aachen, Germany.

26. Amares, A., Sujatmika, E., Hong, T. W., Durairaj, R., and Hamid, H.S.H.B. 2017. A Review: Characteristics of Noise Absorption Material, *Journal of Physics: Conference Series*, **908:** 012005. DOI: 10.1088/1742-6596/908/1/012005.

27. Chelidze, M. (2018). A new simple method for determining the sound absorption coefficient, *MATEC Web conference*, **211:** 04003. DOI: 10.1051/matecconf/201821104003.

28. Deaconu, M., Toma, A. C., Dragasanu, L. I., and Miahai, D. 2017. Comparative Study of Sound Absorption Coefficient Determination Using Fem Method and Experimental Tests on Kundt's Tube, *AIP Conference Proceedings*, **1836:** 020061. DOI: 10.1063/1.4982001.

29. Nandanwar, A., Kiran, M. C., and Varadarajulu, K. Ch. 2017. Influence of Density on Sound Absorption Coefficient of Fibre Board, *Open Journal of Acoustics*, **7:** 1-9. DOI: 10.4236/oja.2017.71001.

30. McGrory, M., Cirac, D. C., Gaussen, O., and Cabrera, D. 2012. Sound absorption coefficient measurement: Re-examining the relationship between impedance tube and reverberant room methods, *Proceeding of Acoustics*, Fremantle, 21-23 November 2012, Australia. Paper Peer Reviewed, Australian Acoustic Society.

31. Wibawa, P.J., Nur, M., Asy'ari, M., and Nur, H. 2020. SEM, XRD and FTIR analyses of both ultrasonic and heat generated activated carbon black microstructures, *Heliyon*, **6(3):** e03546. DOI: 10.1016/j.heliyon.2020.e03546.

32. Ambroz, F.,Macdonald, T. J., Martis, V., and Parkin, I. P. 2018. Evaluation of the BET Theory for the Characterization of Meso and Microporous MOFs, *Small Methods*, **2**: 1800173 (17 pages). DOI: 10.1002/smtd.201800173.

33. Thommes, M., Kaneko, K., Neimark, A. V., Oliver, J. P., Reinoso, F. R-., Rouquerol, J., and Sing, K. S. W. 2015. Physisorption of Gases, with special reference to the evaluation of surface area and pore size distribution (IUPAC Technical Report), *Pure Applied Chemistry*, **87(9-10)**:1051-1069. DOI: 10.1515/pac-2014-1117.

34. Zhang Y., Lam, F. L-. Y., Yan, Z-. F., and Hu- X. 2006. Review of Kelvin's Equation and Its Modification in Characterization of Mesoporous Materials, *Chinese Journal of Chemical Physics*, **19(2)**: 102-108. DOI:10.1360/cjcp2006.19(2).102.7.

35. Parra, J.P., de Sousa, J. C., Bansal, R. C., Pis, J. J., and Pajares, J.A. 1995. Characterization of Activated Carbon by the BET Equation: An Alternative Approach, Book Chapter: *Adsorption Science & Technology*, **12(1)**: 51-66. Multi-Science Publishing, Essex, UK.

36. Coates, J. 2019. In: Meyers, R.A. (Ed.), Interpretation of Infrared Spectra, A Practical Approach, Encyclopedia of Analytical Chemistry. Copyrights John Wiley & Sons Ltd, pp. 123. http://www3.uma.pt/jrodrigues/disciplinas/QINO-II/Teorica/IR.pdf.Online accessed on Wednesday, August 28, 2019 at 08.00 a.m. Indonesian western time.

37. Mistry, B.D. 2009. A Handbook of Spectroscopy Data Chemistry, Edition 2009, p.26-64. Oxford Book Company, Jaypur, India.

38. Silverstein, R. M., Basler, G. C. and Morril, T. C. 1981. Spectrometric Identification of Organic Compounds, 4th. Edition 1981, John Wiley & Sons, New York.

39. Zhu, X., Kim, B-., J., Wang, Q. and Wu, Q. 2014. Recent Advantages in the sound Insulation Properties of Bio-Based Materials, *BioResources*, **9(1)**: 1764-1786. DOI: 10.15376/biores.9.1.1764-1786.

40. Yang, W. D., and Li, Y. 2012. Sound absorption performance of natural fibers and their composites, *Science-China Technological Sciences*, **55(8)**: 2278-2283. DOI: 10.1007/s11431-012-4943-1.

41. Oldham, D.J., Egan, C. A. and Cookson, R. D. 2011. Sustainable acoustic absorbers from the biomass, *Applied Acoustics*, **72(6)**:350-362. DOI: 10.1016/j.apacoust.2010.12.009.

42. Astrauskas, T., Januševičcius, T., and Grubliauskas, R. 2021. Acoustic Panels Made of Paper Sludge and Clay Composites, *Sustainability*, **13**: 637. DOI: 10.3390/su13020637.

43. Koizumi, T., Tsujiuci, N., and Adachi, A. 2002. The development of sound absorbing materials using natural bamboo fibers, *High Performance Structures and Composites*, **4**:157-166. DOI: 10.2495/HPS020161.

44. Xiang, H. F., Wang, D., Liu, H. C., Zhao, N., and Xu, J. 2013. Investigation of sound absorption properties of kapok fibers, *Chinese Journal of Polymer Science*, **31(3)**: 521-529. DOI: 10.1007/s10118-013-1241-8.

45. Cao, L., Fu, Q., Si, Y., Ding, B., and Yu, J. 2018. Short Review: Porous materials for sound absorption, *Composites Communications*, **10**: 25–35. DOI: 10.1016/j.coco.2018.05.001.
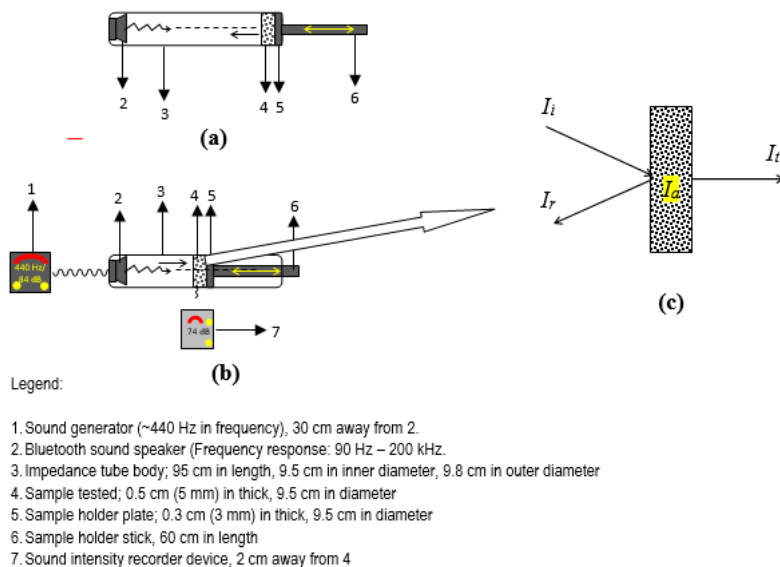
Figures

Legend:

1. Sound generator (~440 Hz in frequency), 30 cm away from 2.
2. Bluetooth sound speaker (Frequency response: 90 Hz – 200 kHz.
3. Impedance tube body; 95 cm in length, 9.5 cm in inner diameter, 9.8 cm in outer diameter
4. Sample tested; 0.5 cm (5 mm) in thick, 9.5 cm in diameter
5. Sample holder plate; 0.3 cm (3 mm) in thick, 9.5 cm in diameter
6. Sample holder stick, 60 cm in length
7. Sound intensity recorder device, 2 cm away from 4

Figure 1

Schematic illustration of the sound adsorbtion test equipment of the fabricated WHBC-PVA composite using a modified impedance tube, (a) Impedance tube before sound exposure, here the distance between sound speaker 2 and sound absorber material tested 4 was 92 cm, (b) Impedance tube during sound exposure, here the distance between sound speaker 2 and sound absorber material tested 4 was 41 cm, and (c) Simplification of the sound absorption track,

i.e., $I_a = I_i - I_r - I_t$ where I_a, I_i, I_r, and I_t is sound absorbed, sound incident, reflected sound, and transmitted sound respecively, in intesity each. Here, I_i was 84 dB, while I_r and I_t was assumed totally recorded simultaneously by the sound recorder device, marked 7.
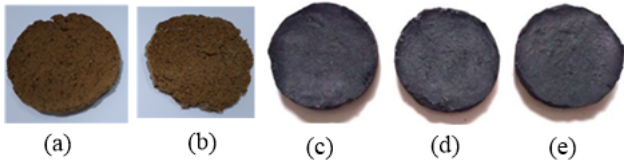

(a)   (b)   (c)   (d)   (e)

Figure 2

Photograph of several products of the WHBC materials, (a) WHori1; (b) WHori2; (c) WHBC400-PVA; (d) WHBC500-PVA; (e) WHBC600-PVA. The size of each is 9 cm diameter, and 0.5 cm thick.
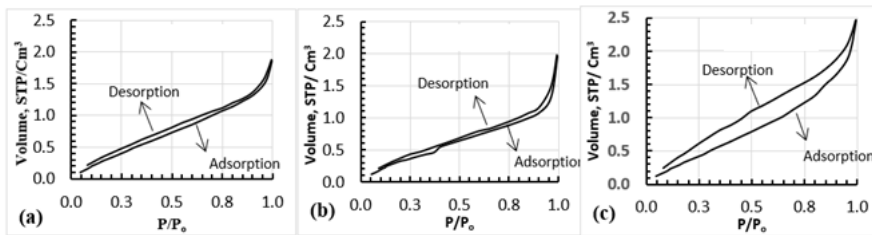
Figure 3

Isotherm adsorption types of the WHBC-PVA composites encode as (a) WHBC400-PVA, (b) WHBC500-PVA, (c) WHBC600-PVA
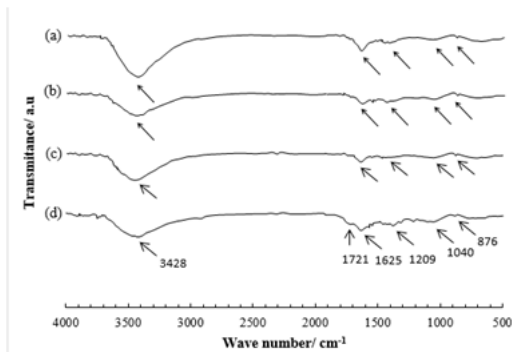

Figure 4

FTIR spectra of the fabricated WHBC-PVA composites of (a) WHBC400-PVA, (b) WHBC500-PVA, and (c) WHBC600-PVA, while (d) WHBC original
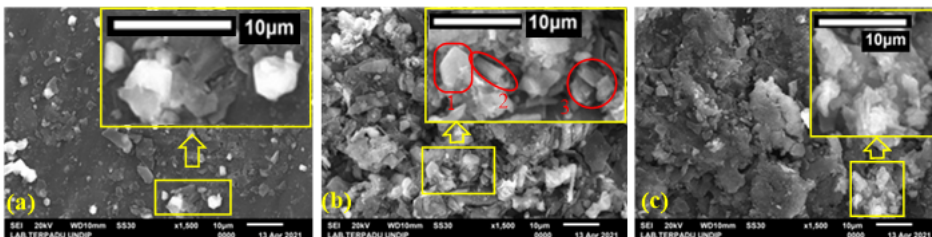

Figure 5

SEM images of the fabricated WHBC-PVA composites of (a) WHBC400-PVA, (b) WHBC500-PVA, and (c) WHBC600-PVA, each with 1500 ´ magnification.

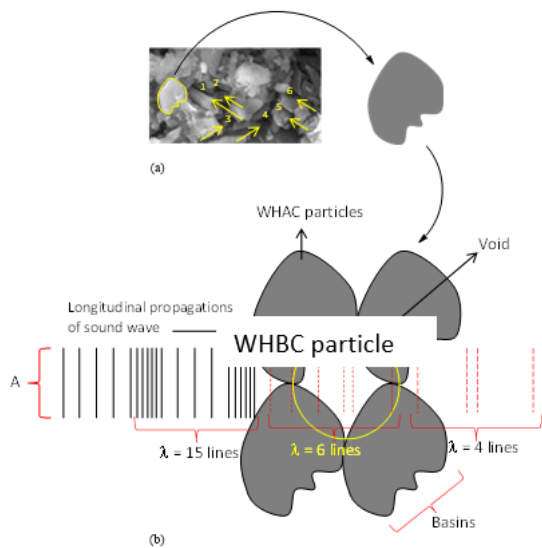Inset are 400 larger zooms out of its associated image.

Figure 6

(a) Inset of the SEM images Figure 5(b), here one particle of WHBC500 materials was taken to construct an illustration of a void by using four such particles. While 1,2,3,4,5, and 6 marks are real several voids are constructed by some different shapes of particles. (b) Schematic illustration of the mechanism of the sound absorption process passed through the WHBC500 material, expressed as reduction of sound frequency.

Supplementary Files

This is a list of supplementary files associated with this preprint. Click to download.

- SupplementaryMaterialS1S14Revision.docx
- SupportingInformationFTIRinExcelformatRevision.xlsx